The Astrophysical Journal, 660:276–287, 2007 May 1

DENSITY STRUCTURE OF THE INTERSTELLAR MEDIUM AND THE STAR FORMATION RATE IN GALACTIC DISKS

Keiichi Wada[1]
National Astronomical Observatory of Japan, Mitaka, Tokyo 181-8588, Japan; wada.keiichi@nao.ac.jp

and

Colin A. Norman[2]
Department of Physics and Astronomy, Johns Hopkins University, Baltimore, MD 21218; norman@pha.jhu.edu
Received 2006 May 8; accepted 2007 January 19

ABSTRACT

The probability distribution functions (PDFs) of the density of the interstellar medium (ISM) in galactic disks and the global star formation rate (SFR) are discussed. Three-dimensional hydrodynamic simulations show that the PDFs in a globally stable, inhomogeneous ISM in galactic disks are well fitted by a single lognormal function over a wide density range. The dispersion of the lognormal PDF (LN-PDF) is larger for more gas-rich systems, whereas the characteristic density of the LN-PDF, for which the volume fraction becomes the maximum, does not significantly depend on the initial conditions. Supposing the galactic ISM is characterized by the LN-PDF, we give a global SFR as a function of average gas density, a critical local density for star formation, and the star formation efficiency (SFE). Although the present model is more appropriate for massive and geometrically thin disks ($\sim$10 pc) in inner galactic regions (<a few kpc), we can make a comparison between our model and observations in terms of the SFR, provided that the LN nature of the density field is also the case in the real galactic disk with a large scale height ($\sim$100 pc). We find that the observed SFR is well-fitted by the theoretical SFR over a wide range of the global gas density (10–$10^4\, M_\odot$ pc^{-2}). The star formation efficiency (SFE) for high-density gas ($n > 10^3$ cm^{-3}) is SFE $= 0.001$–0.01 for normal spiral galaxies and 0.01–0.1 for starburst galaxies. The LN-PDF and SFR proposed here could be applicable for modeling star formation on a kiloparsec scale in galaxies or numerical simulations of galaxy formation, in which the numerical resolution is not fine enough to describe the local star formation.

Subject headings: galaxies: starburst — ISM: kinematics and dynamics — ISM: structure — methods: numerical

1. INTRODUCTION

The ISM in galaxies is characterized by a highly inhomogeneous structure with a wide variety of physical and chemical states (Myers 1978). Stars are formed in this complexity through gravitational instability in molecular cores, but the entire multiphase structure on a global scale is quasi-stable. It is therefore important to understand theoretically the structure of the ISM over a wide dynamic range to model star formation in galaxies. Observations suggest that there is a positive correlation between the global SFR and the average gas density: $\dot{\Sigma}_\star \propto \Sigma_{\rm gas}^N$, with $N \sim 1.4$ in nearby galaxies (Kennicutt 1998).[3] Since the star formation process itself is a local phenomenon on a subparsec scale, the observed correlation between the structure of the ISM on a local scale and the global quantities, such as the average gas density, implies that the ISM on different scales is physically related.

In fact, two- (2D) and three-dimensional (3D) hydrodynamic and magnetohydrodynamic simulations (e.g., Bania & Lyon 1980; Vázquez-Semadeni et al. 2000; Rosen & Bregman 1995; de Avillez 2000) show that there is a robust relation between the local and global structures of the multiphase ISM, which is described by an LN density PDF. Elmegreen (2002) first noticed that if the density PDF is LN and star formation occurs in dense gases above a critical density, the Schmidt-Kennicutt law is reproduced. This provides a new insight on the origin of the scaling relation. More recently, Krumholz & McKee (2005) give a similar model for the SFR in molecular clouds. In these theoretical predictions, the dispersion of the LN-PDF, σ, is a key parameter. Elmegreen (2002) used $\sigma = 2.4$, which is taken from 2D hydrodynamic simulations of the ISM (Wada & Norman 2001, hereafter WN01). Krumholz & McKee (2005) assumed an empirical relation between σ and the rms Mach number, which is suggested in numerical simulations of isothermal turbulence (see also § 4.1). Therefore, it is essential to know whether the LN-PDF in galactic disks is universal and what determines σ. However, most previous simulations, in which the LN-PDF or the power-law PDF are reported, are "local" simulations: a patch of the galactic disk is simulated with a periodic boundary condition. Apparently, such local simulations are not suitable for discussing the statistical nature of the ISM in galactic disks. For example, the number of density condensations is not large enough (typically a few) (see Scalo et al. 1998; Slyz et al. 2005).

On the other hand, global hydrodynamic simulations for 2D galactic disks or 3D circumnuclear gas disks suggested that the density PDF, especially a high-density part, is well fitted by a single LN function over 4–5 decades (Wada & Norman 1999; WN01; Wada 2001, hereafter W01). The LN-PDF is also seen in a high-z galaxy formed by a cosmological N-body/adaptive mesh refinement (AMR) simulation (Kravtsov 2003). Nevertheless,

[1] Department of Astronomical Science, Graduate University for Advanced Studies, Mitaka, Tokyo 181-8588, Japan.

[2] Space Telescope Science Institute, Baltimore, MD 21218.

[3] Recent observations reported a wide range for the slope, e.g., $N \sim 1.1$ or 1.7, depending on the extinction models (Wong & Blitz 2002). Komugi et al. (2005) found that $N \sim 1.33$ for the central part of normal galaxies, and they also suggest that the SFR is systematically lower than those in starburst galaxies (see also § 3.3).

TABLE 1
INITIAL DENSITY AND FITTING PARAMETERS OF THE DENSITY PDF

Model	ρ_i[a] ($M_\odot$ pc^{-3})	σ_{10}[b]	σ[c]	log ρ_0[d]	α[e]	$\sigma_{10,M}$[f]	σ_M[g]	σ_p[h]
A	5	1.025	2.360	−1.40	0.09	1.025	2.360	2.483
B	10	1.188	2.735	−1.55	0.12	1.188	2.735	2.769
C	15	1.223	2.816	−1.60	0.18	1.273	2.849	2.810
D	50	1.308	3.012	−1.50	0.20	1.308	3.012	3.104

[a] Initial density.
[b] Dispersion of volume-weighted LN-PDF (eq. [5]).
[c] $\sigma \equiv \sigma_{10}$ ln 10.
[d] The reference density for the volume-weighted PDF (eq. [5]). The unit of density is $M_\odot$ pc^{-3}.
[e] Volume fraction of the LN part (eq. [5]).
[f] Dispersion of mass-weighted LN-PDF (Fig. 9).
[g] $\sigma_M \equiv \sigma_{10,M}$ ln 10. If the PDF is a perfect LN, $\sigma = \sigma_M$.
[h] Dispersion of LN-PDF predicted from eq. (14).

the universality of the LN-PDF and how it is related to global quantities are still unclear.

In this paper, we verify the LN nature of the ISM in galactic disks, using 3D, global hydrodynamic simulations. This is an extension of our previous 2D studies of the ISM in galactic disks (WN01) and 3D model of the galactic central region (Wada & Norman 2002). We confirm that the dispersion σ of the LN function is related to the average gas density of the disk. We then calculate the SFR as a function of critical density of the local star formation and the SFE. This is a generalized version of the Schmidt law (Schmidt 1959), and it can be applied to various situations.

An alternative way to study the global SFR in galaxies is simulating star formation directly in numerical models (e.g., Li et al. 2006; Kravtsov & Gnedin 2005; Tasker & Bryan 2006). In this approach, "stars" are formed according to a "star formation recipe," and the resulting SFR is compared to observations. We do not use this methodology, because numerical modeling of star formation in simulations still requires many free parameters and assumptions. Moreover, if the numerically obtained SFR deviates from the observed scaling relation (this is usually the case; see, e.g., Tasker & Bryan 2006), it is hard to say what we can learn from the results. This deviation might be due to wrong implementation of star formation in the numerical code, or the estimate of the SFR in observations might be wrong, since the SFR is not directly observable. One should also realize that comparison with observations of local galaxies is not necessarily useful when we discuss the SFR in different situations, such as galaxy formation. In this paper, we avoid the ambiguity in terms of star formation in simulations and alternatively discuss the SFR based on an intrinsic statistical feature of the ISM. The effect of energy feedback from supernovae is also discussed.

This paper is organized as follows. In § 2, we describe results of numerical simulations of the ISM in a galactic disk, focusing on the PDF. In § 3, we start from a "working hypothesis," that is, the inhomogeneous ISM, which is formed through nonlinear development of density fluctuations and is characterized by a LN density PDF. After summarizing basic properties of the LN-PDF, we use the LN-PDF to estimate a global SFR, and it is compared with observations. In § 4, we discuss implications of the results in §§ 2 and 3. In order to distinguish local (i.e., subparsec-scale) and global (i.e., galactic-scale) phenomena, we basically use cm^{-3} for local number density and $M_\odot$ pc^{-3} (or $M_\odot$ pc^{-2}) for global density.[4]

[4] The density 1 $M_\odot$ pc$^{-3} \simeq 66.7$ cm^{-3}, if the mean weight of a particle is $0.61 m_{\rm H}$.

2. GLOBAL SIMULATIONS OF THE ISM IN GALACTIC DISKS AND THE PDF

2.1. *Numerical Methods*

Evolution of rotationally supported gas disks in a fixed (i.e., time-independent), spherical galactic potential is investigated using 3D hydrodynamic simulations. We take into account self-gravity of the gas, and radiative cooling and heating processes. The numerical scheme is an Euler method with a uniform Cartesian grid, which is based on the code described in WN01 and W01. Here we briefly summarize them. We solve the conservation equations and Poisson equation in three dimensions:

$$\frac{\partial \rho}{\partial t} + \nabla \cdot (\rho \boldsymbol{v}) = 0, \tag{1}$$

$$\frac{\partial \boldsymbol{v}}{\partial t} + (\boldsymbol{v} \cdot \nabla)\boldsymbol{v} + \frac{\nabla p}{\rho} + \nabla \Phi_{\rm ext} + \nabla \Phi_{\rm sg} = 0, \tag{2}$$

$$\frac{\partial (\rho E)}{\partial t} + \nabla \cdot [(\rho E + p)\boldsymbol{v}] = \rho \Gamma_{\rm UV} + \Gamma_{\rm SN} - \rho^2 \Lambda(T_g), \tag{3}$$

$$\nabla^2 \Phi_{\rm sg} = 4\pi G \rho, \tag{4}$$

where ρ, p, and $\boldsymbol{v}$ are the density, pressure, and velocity of the gas, respectively. The specific total energy $E \equiv |\boldsymbol{v}|^2/2 + p/(\gamma - 1)\rho$, with $\gamma = 5/3$. The spherical potential is $\Phi_{\rm ext} \equiv -(27/4)^{1/2} \times [v_1^2/(r^2 + a_1^2)^{1/2} + v_2^2/(r^2 + a_2^2)^{1/2}]$, where $a_1 = 0.3$ kpc, $a_2 = 5$ kpc, and $v_1 = v_2 = 200$ km s^{-1}. We also assume a cooling function $\Lambda(T_g)$ (10 K $< T_g < 10^8$ K) (Spaans & Norman 1997) with solar metallicity. We assume photoelectric heating by dust and a uniform UV radiation field, $\Gamma_{\rm UV} = 1.0 \times 10^{-23} \varepsilon G_0$ ergs s^{-1}, where the heating efficiency ε is assumed to be 0.05 and G_0 is the incident far-UV field normalized to the local interstellar value (Gerritsen & Icke 1997). In order to focus on a intrinsic inhomogeneity in the ISM due to gravitational and thermal instability, at first we do not include energy feedback from supernovae. In § 4.5 we show a model with energy feedback from supernovae (i.e., $\Gamma_{\rm SN} \neq 0$). Note that even if there is no random energy input from supernovae, turbulent motion can be maintained in the multiphase, inhomogeneous gas disk (Wada et al. 2002).

The hydrodynamic part of the basic equations is solved by AUSM (Advection Upstream Splitting Method; Liou & Steffen 1993) with a uniform Cartesian grid. We achieve third-order spatial accuracy with MUSCL (Monotone Upstream-centered Schemes for Conservation Laws; van Leer 1979). We use $512 \times 512 \times 64$ grid points covering a $2.56 \times 2.56 \times 0.32$ kpc^3 region (i.e., the spatial resolution is 5 pc). For comparison, we also run models with a

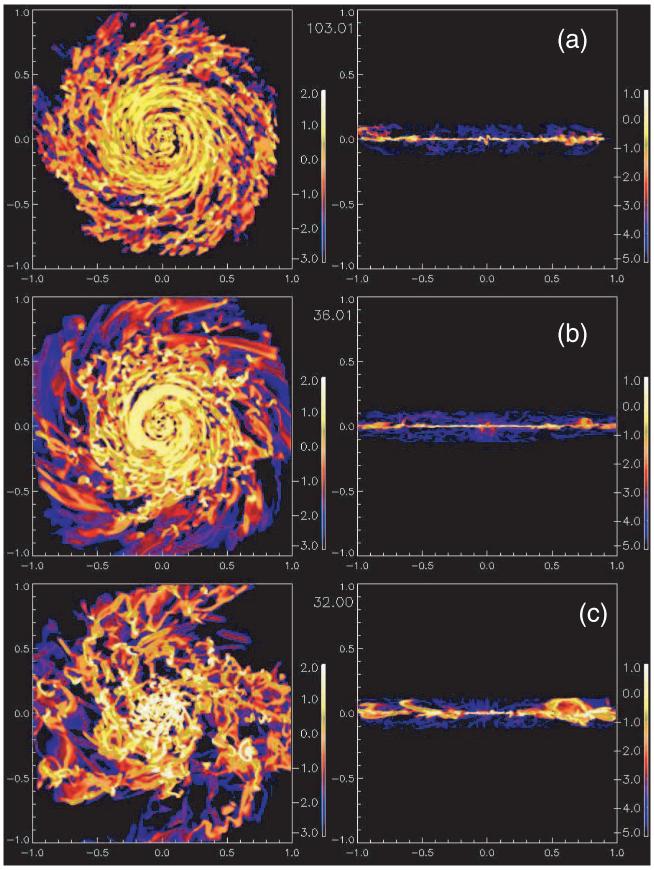

FIG. 1.— Surface sections of the density distribution of the gas in models with different initial density (models A, B, and D). The *x-y* and *x-z* planes are shown. The unit of length is kiloparsecs. (*a*) Model A ($\rho_i = 5\ M_\odot$ pc^{-3}, $t = 103$ Myr), (*b*) model B ($\rho_i = 10\ M_\odot$ pc^{-3}, $t = 36$ Myr), and (*c*) model D ($\rho_i = 50\ M_\odot$ pc^{-3}, $t = 32$ Myr).

10 pc resolution. The Poisson equation is solved to calculate self-gravity of the gas using the fast Fourier transform (FFT) and the convolution method (Hockney & Eastwood 1981). In order to calculate the isolated gravitational potential of the gas, the FFT is performed for a working region of $1024 \times 1024 \times 128$ grid points (see details in WN01). We adopt implicit time integration for the cooling term. We set the minimum temperature, for which the Jeans instability can be resolved with a grid size Δ, namely, $T_{\rm min} = 35$ K $(\rho/10\ M_\odot\ {\rm pc}^{-3})(\Delta/5\ {\rm pc})^2$.

The initial condition is an axisymmetric and rotationally supported thin disk (scale height is 10 pc) with a uniform density ρ_i. We run four models with different ρ_i (see Table 1). Random density and temperature fluctuations are added to the initial disk. These fluctuations are less than 1% of the unperturbed values and have an approximately white noise distribution. The initial temperature is set to 10^4 K over the whole region. At the boundaries, all physical quantities remain at their initial values during the calculations.

2.2. *Numerical Results*

Figure 1 is snapshots of density distribution at a quasi-stable state for models A, B, and D on the *x-y* and *x-z* planes. Depending on the initial density ($\rho_i = 5$, 10, and 50 $M_\odot$ pc^{-3}), distribution of the gas in a quasi-equilibrium is different. In the most massive disk (Fig. 1*c*, model D), the disk is fragmented into clumps and filaments; on the other hand, the less massive disk (Fig. 1*a*, model A) shows a more axisymmetric distribution with tightly winding spirals and filaments. In Figure 2, we show vertical structures of density of model D ($t = 42$ Myr). The high-density disk ($\rho > 0.1\ M_\odot$ pc^{-3}) is resolved by about 10 grid points out of 64 total grid points for the *z*-direction. A density change of about 5 orders of magnitude from the disk to halo gas is resolved.

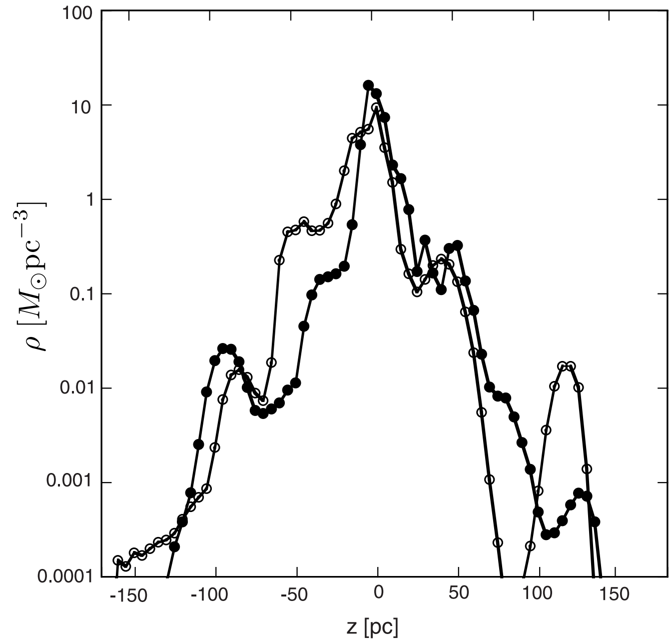

FIG. 2.—Vertical density structure of model D. The two lines represent density averaged for the *x*- (*filled circles*) and *y*-direction (*open circles*).

Figure 3 is the time evolution of a density PDF in model D. The initial uniform density distribution, which forms a peak around $\rho \simeq 50\ M_\odot$ pc^{-3}, is smoothed out in ~10 Myr, and becomes a smooth distribution in ~20 Myr. Figure 4 shows PDFs spatially deconvolved to four components (thin disk, thick disk in the inner disk, halo, and the whole computational box; see figure caption for definitions) of model D in a quasi-steady state ($t = 32$ Myr). It is

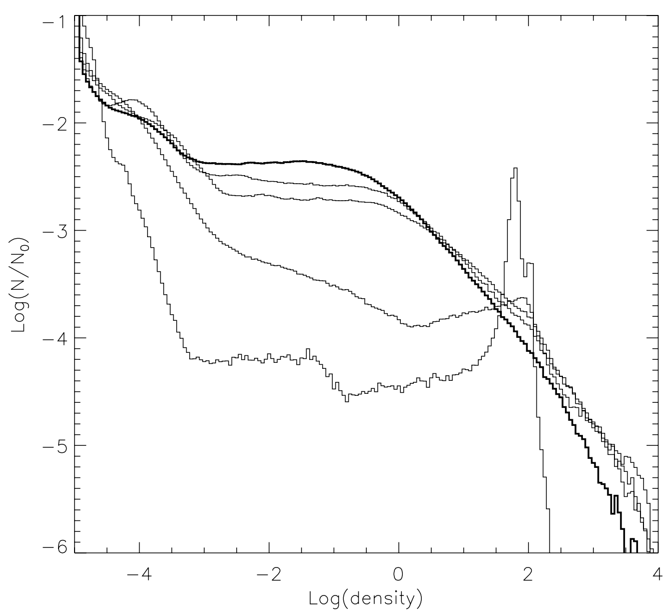

FIG. 3.—Time evolution of density PDF for the whole computational volume for model D. The lines represent the PDF at $t = 3$, 10, 16, 21, and 43 Myr (*thick solid line*). The vertical axis is the number fraction of grid cells for the density. The unit of density is $M_\odot$ pc^{-3}.

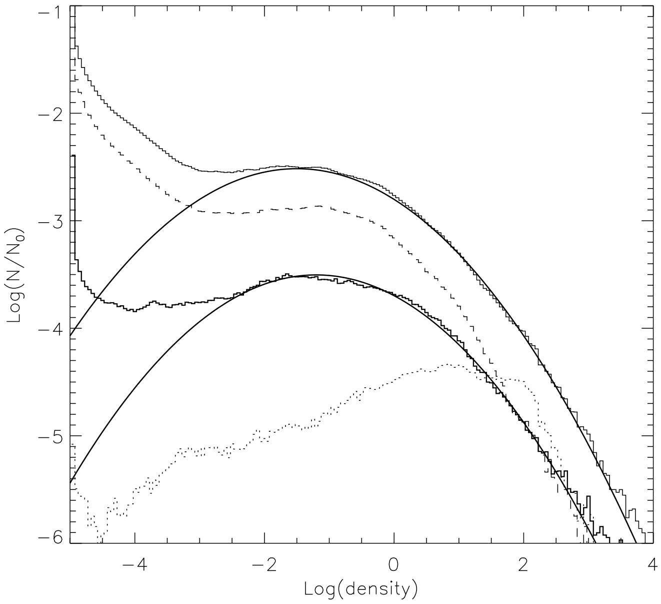

FIG. 4.—Density PDF for four subregions in model D. The solid line is a thin disk ($|z| \leq 10$ pc), the dotted line is an inner disk (10 pc $\leq z \leq$ 20 pc and $|x, y| \leq 0.38$ kpc), and the dashed line is a halo (30 pc $\leq z \leq$ 160 pc), where $z = 0$ is the galactic plane. The two solid curves are an LN function with $\sigma_{10} = 1.273$, $\log(\rho_0) = -1.2$, and $\alpha = 0.02$ (disk), and $\sigma_{10} = 1.308$, $\log(\rho_0) = -1.5$, and $\alpha = 0.2$ (the whole region).

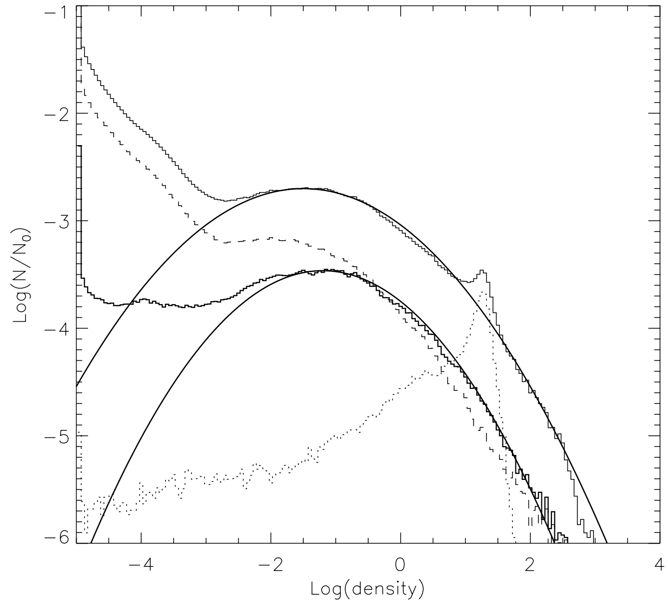

FIG. 5.—Same as Fig. 4, but for model B.

clear that dense regions ($\rho \gtrsim 0.01\ M_\odot$ pc^{-3}) can be fitted by a single LN function, $f_{\rm LN}$, over nearly six decades:

$$f_{\rm LN}(\rho; \rho_0, \sigma_{10}) = \frac{\alpha}{\sqrt{2\pi}\sigma_{10} \ln 10} \exp\left[-\frac{\log(\rho/\rho_0)^2}{2\sigma_{10}^2}\right], \quad (5)$$

where α is the volume fraction of the high-density part, which is fitted by the LN-PDF. On a galactic scale, the ISM is multiphase, and dense, cold gases occupy smaller volumes than diffuse, hot gases. Therefore, it is reasonable that the density PDF shows a negative slope against density, as shown in the previous numerical simulations. However, our results suggest that the structure of the ISM is not scale-free. The LN-PDF implies that the formation process for the high-density part is highly nonlinear (Vázquez-Semadeni 1994). High-density regions can be formed by convergent processes, such as mergers or collisions between clumps/filaments, or compressions by sound waves or shock waves. Tidal interaction between clumps, galactic shear, or local turbulent motion can also change their density structure. For a large enough volume, and for a long enough period, these processes can be regarded as many random, independent processes in a galactic disk. In this situation, the density in a small volume is determined by a large number of independent random events, which can be expressed by $\rho = \Pi_{i=1}^{i=N} \delta_i \rho_s$ with independent random factors δ_i and initial density ρ_s. Therefore, the distribution function of $\log(\rho)$ should be Gaussian according to the central limit theorem, if $N \to \infty$.

In Table 1, we summarize fitting results for the PDF in the four models in terms of the whole volume. One important result is that there is a clear trend that the dispersion is larger for more massive systems. The less massive model (model B) also shows a LN-PDF (Fig. 5), but the dispersion is smaller ($\sigma_{10} = 1.188$) than that in model D. The PDF for the whole volume is LN, but there is a peak around $\log \rho = 1.3$. As shown by the dotted line, this peak comes from the gas just above the disk plane (10 pc $\leq z \leq$ 20 pc) in the inner disk ($r \lesssim 0.38$ kpc), where the gas is dynamically stable, and therefore the density is not very different from its initial value ($\rho_i = 10$). This peak is not seen in the dotted line in model D (Fig. 4), since the density field in model D is not uniform even in the inner region due to the high initial density.

The excess of the volume at low density ($\lesssim 10^{-3}\ M_\odot$ pc^{-3}; see Figs. 4 and 5) is due to a smooth component that is extended vertically outside the thin, dense disk. About 10%–20% of the whole computational box is in the LN regime (i.e., $\alpha = 0.1$–0.2). However, most mass is in the LN regime (see Fig. 9).

In order to ensure that gravitational instability in the high-density gas is resolved, we set a minimum temperature $T_{\rm min}$, which depends on the grid size (§ 2.1). We run model C with two different resolutions, 5 and 10 pc. As seen in Figure 6, although the "tangled web" structure is qualitatively similar between the two models,

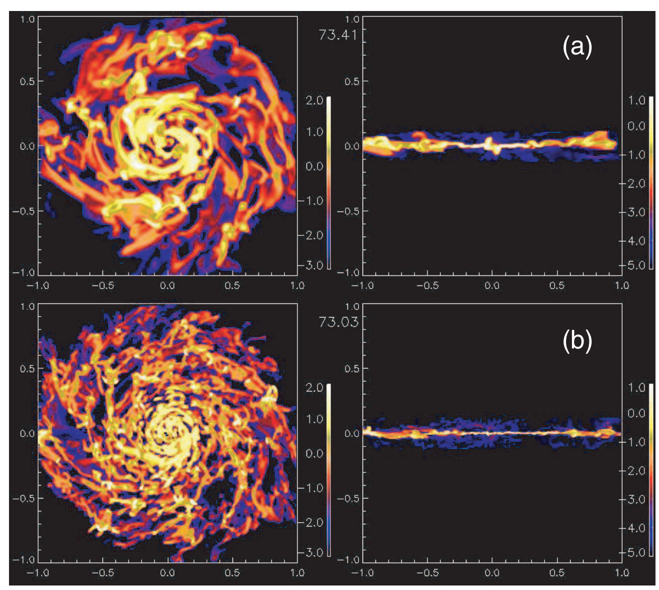

FIG. 6.—Density structures of model C with two different resolutions and a temperature floor depending on the resolution: (*a*) $\Delta = 10$ pc and (*b*) $\Delta = 5$ pc. The criterion $T_{\rm min} = 35$ K $[\rho_i/(10\ M_\odot\ {\rm pc}^{-3})](\Delta/5\ {\rm pc})^2$ is assumed to ensure that the Jeans instability is resolved.

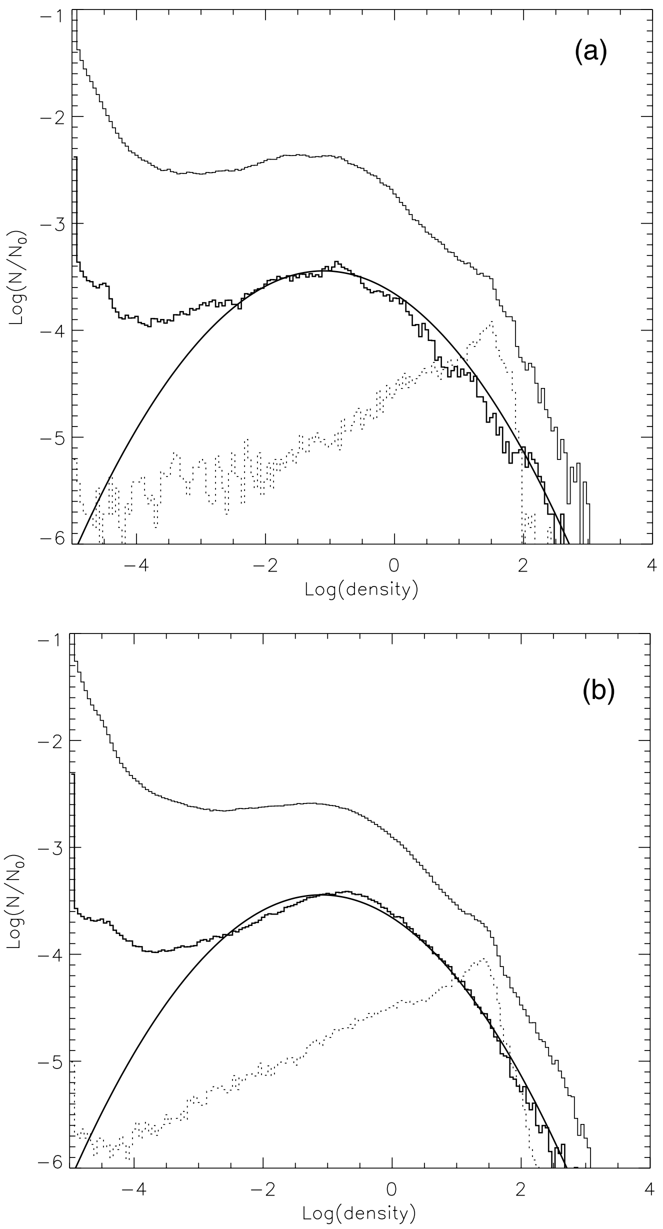

FIG. 7.—Density PDF for model C with two different resolutions: (*a*) $\Delta = 10$ pc and (*b*) $\Delta = 5$ pc. The three lines are the PDFs for the whole computational box (*top line*), the disk (*fitted by an LN-PDF*), and the inner disk (*dotted line*).

the typical scales of the inhomogeneity, for example, the width of the filaments, are different. The scale height of the disk H in the model with $\Delta = 5$ pc is about a factor of 2 smaller than the model with $\Delta = 10$ pc. This is reasonable, since $T_{\rm min} \propto \Delta^2$ and $H \propto T_g^{1/2}$, if the disk is vertically in hydrostatic equilibrium. In Figure 7, we compare density PDFs in the two models with different spatial resolution. PDFs in the models are qualitatively similar, in a sense that the PDF has a LN part for high-density gas, although the PDF in the model with a 10 pc resolution is not perfectly fitted by a LN function. This comparison implies that the spatial resolution should be at least 5 pc in order to discuss the PDF of the ISM in galactic disks.

Figure 8 shows a phase diagram of model D. Three dominant phases in volume, i.e., hot ($T_g \sim 10^5$ K), warm ($T_g \sim 8000$ K), and cold gas ($T_g \sim 30$–1000 K), exist. The temperature of the gas denser than $\rho \simeq 10\ M_\odot$ pc^{-3} is limited by $T_{\rm min}$. As suggested by Figure 8, the frequency distribution of temperature is not

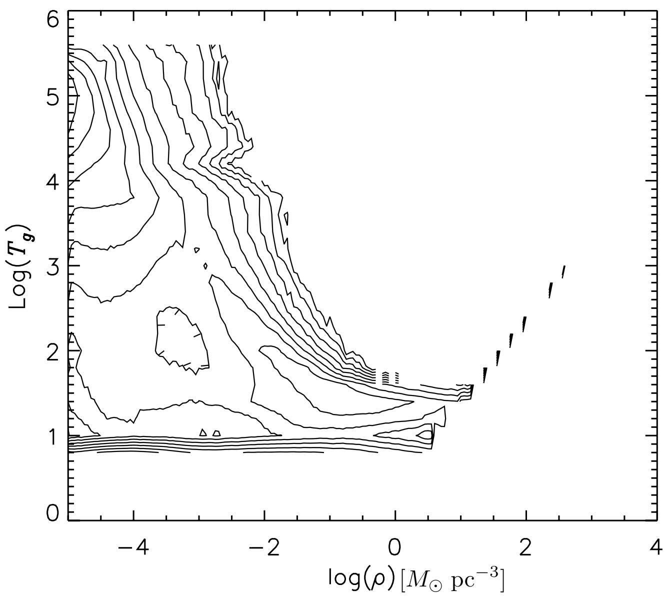

FIG. 8.—Phase diagram of model D at $t = 43$ Myr. Contours represent log-scaled volumes.

represented by a single smooth function, which is a notable difference from the density PDF. High-density gas ($\rho > 10^{-2}\ M_\odot$ pc^{-3}) is not isothermal, suggesting that isothermality is not a necessary condition for the LN density PDF in global models of the ISM (see also § 4.1).

As qualitatively seen in Figure 1, the dispersion of the LN-PDF is larger in a more massive system. This is seen more quantitatively in Figure 9, which shows mass-weighted PDFs in four models with different ρ_i. In the fit, we use the same σ obtained from the volume-weighted PDF, and the mass-weighted characteristic density $\rho_{0,M}$ is calculated using

$$\rho_{0,M} = \rho_0 e^{\sigma^2}. \quad (6)$$

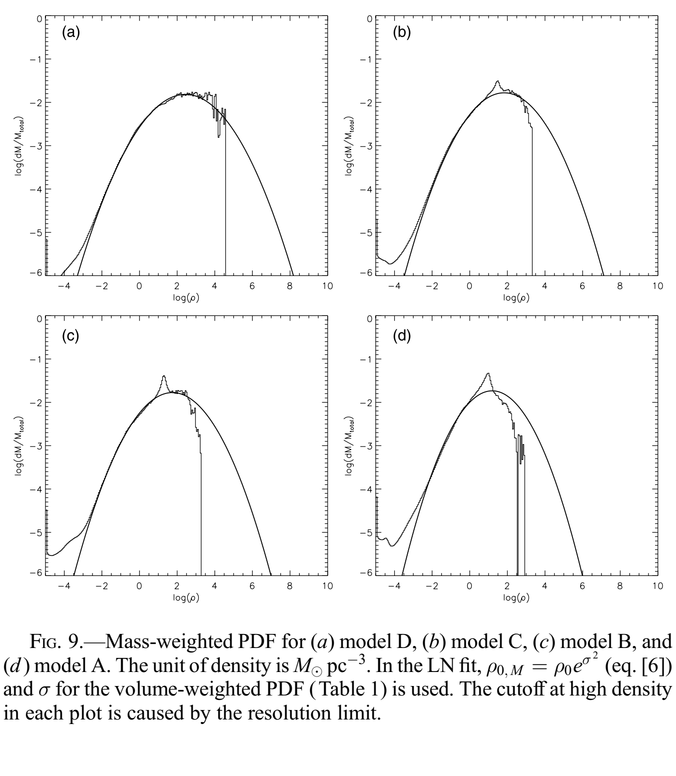

FIG. 9.—Mass-weighted PDF for (*a*) model D, (*b*) model C, (*c*) model B, and (*d*) model A. The unit of density is $M_\odot$ pc^{-3}. In the LN fit, $\rho_{0,M} = \rho_0 e^{\sigma^2}$ (eq. [6]) and σ for the volume-weighted PDF (Table 1) is used. The cutoff at high density in each plot is caused by the resolution limit.

Equation (6) is always true if the PDF is LN. The dispersion σ is 2.36 in model A ($\rho_i = 5\ M_\odot$ pc^{-3}) and 3.01 in model D ($\rho_i = 50\ M_\odot$ pc^{-3}) (Table 1). The dependence of σ on the initial gas density (or total gas mass) is a natural consequence of the LN-PDF (see § 3.1). From comparison between the volume-weighted and the mass-weighted PDF, it is clear that even if the smooth non-LN regime occupies most of the volume of the galactic disk–halo region (i.e., $\alpha < 1$), the mass of the ISM is dominated by the LN-PDF regime.

Another important point in the numerical results is that the characteristic density of the LN-PDF, ρ_0, does not significantly change among the models, despite the wide (almost 8 orders of magnitude) density range in the quasi-steady state. In fact, as shown in Table 1, ρ_0 is in the range 1.7 cm^{-3} $< \rho_0 <$ 2.7 cm^{-3} among the models with $\rho_i = 5$–$50\ M_\odot$ pc^{-3}. The physical origin of this feature is discussed in § 3.1.

In summary, using our 3D high-resolution hydrodynamic simulations, we find that the ISM in a galactic disk is inhomogeneous on a local scale, and it consists of many filaments, clumps, and low-density voids, which are in a quasi-steady state on a global scale. The statistical structure of the density field in the galactic disk is well described by a single LN-PDF over six decades in a high-density part (i.e., $\rho \gtrsim 0.01\ M_\odot$ pc^{-3}). Most of the mass is in the regime of the LN-PDF. The dispersion of the LN-PDF is larger for more massive systems.

3. PDF AND THE SFR

3.1. *Basic Properties of the LN-PDF*

In this section, based on the properties of the LN-PDF, we discuss how we can understand the numerical results in § 2. Suppose that the density PDF, $f(\rho)$, in the galactic disk is described by a single LN function:

$$f(\rho)\,d\rho = \frac{1}{\sqrt{2\pi}\sigma}\exp\left[-\frac{\ln(\rho/\rho_0)^2}{2\sigma^2}\right]d\ln\rho, \tag{7}$$

where ρ_0 is the characteristic density and σ is the dispersion. The volume-averaged density $\langle\rho\rangle_V$ for the gas described by the LN-PDF is then

$$\langle\rho\rangle_V = \frac{1}{\sqrt{2\pi}\sigma}\int_{-\infty}^{\infty}\rho\exp\left[-\frac{\ln(\rho/\rho_0)^2}{2\sigma^2}\right]d\ln\rho, \tag{8}$$

$$= \rho_0 e^{\sigma^2/2}. \tag{9}$$

The mass-averaged density is

$$\langle\rho\rangle_M \equiv \frac{\int\rho^2\,dV}{M_t} = \rho_{0,M}e^{\sigma^2} = \rho_0 e^{2\sigma^2}, \tag{10}$$

where $M_t = \int\rho\,dV$ is the total mass in the LN regime. The dispersion σ of the LN-PDF is therefore

$$\sigma^2 = \frac{2}{3}\ln\left(\frac{\langle\rho\rangle_M}{\langle\rho\rangle_V}\right). \tag{11}$$

Equivalently, using ρ_0,

$$\sigma^2 = 2\ln\left(\frac{\langle\rho\rangle_V}{\rho_0}\right) \tag{12}$$

$$= \frac{1}{2}\ln\left(\frac{\langle\rho\rangle_M}{\rho_0}\right). \tag{13}$$

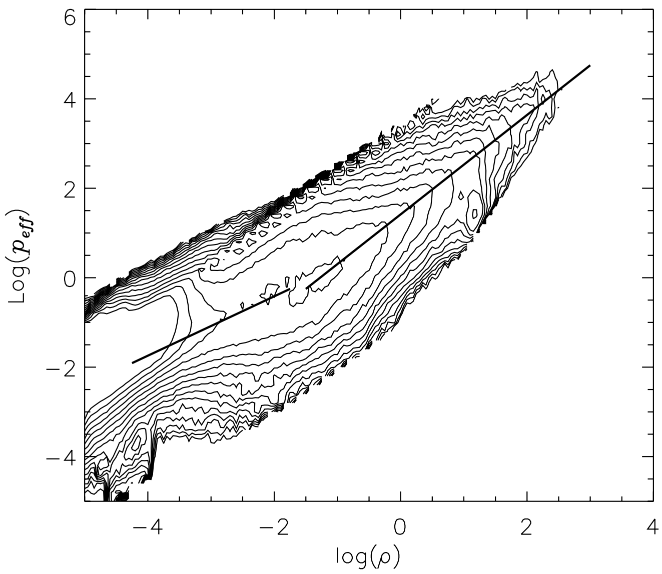

FIG. 10.—Effective pressure–density diagram of model E. The two power laws are $p_{\rm eff} \propto \rho^{2/3}$ and $p_{\rm eff} \propto \rho^{4/3}$. Here, $p_{\rm eff} \equiv p_{\rm th} + \rho v_t^2$, where $p_{\rm th}$ is the thermal pressure and v_t is the turbulent velocity of the medium. The contours represent log-scaled volumes for given density and $p_{\rm eff}$.

Suppose the characteristic density ρ_0 is nearly constant, as suggested by the numerical results, Equations (12) or (13) tells us that the dispersion σ is larger for more massive systems, which is also consistent with the numerical results. For a stable, uniform system, i.e., $\langle\rho\rangle_V = \rho_0$, σ should be zero. In another extreme case, namely, $\langle\rho\rangle_V \to \infty$, $\sigma \to \infty$, but this is not the case, because the system itself is no longer dynamically stable. Therefore, σ should take a number in an appropriate range in globally stable, inhomogeneous systems. Galactic disks are typical examples of such systems.

In our numerical results, the ISM with a low-density part (typically less than $10^{-3}\ M_\odot$ pc^{-3}) is not fitted by the LN-PDF. If the density field of the ISM in a fraction, α, of the volume of the density field is characterized by the LN-PDF, the volume-averaged density in the volume is $\bar{\rho} = \alpha\langle\rho\rangle_V$. In this case, equation (12) is modified to

$$\sigma_p^2 = 2\ln\left(\frac{\bar{\rho}}{\alpha\rho_0}\right). \tag{14}$$

As shown in Table 1, σ in the numerical results agrees well with σ_p in each model. In numerical simulations, it is easy to know the volume in the LN-regime (i.e., $\alpha\times$volume of the computational box); therefore, calculating σ_p is straightforward using equation (14). However, if one wants to evaluate σ from observations of galaxies, it is more practical to use the mass-averaged density, equation (13), because it is expected that the mass of the galactic ISM is dominated by the LN regime in mass (see Fig. 9).

Interestingly, even if the density contrast is extremely large (e.g., 10^6–10^8), the numerical results show that the characteristic density ρ_0 is not sensitive for the total gas mass in a kiloparsec galactic disk ($\rho_0 = 1.7$–2.7 cm^{-3}). If this is the case, what determines ρ_0? In Figure 10, we plot effective pressure, $p_{\rm eff} \equiv p_{\rm th} + \rho v_t^2$, as a function of density, where $p_{\rm th}$ is the thermal pressure and v_t is the turbulent velocity dispersion, which is obtained by averaging the velocity field in each subregion with a (10 pc)^3 volume. If the turbulent motion in a volume with a size L originates in self-gravity of the gas and galactic rotation (Wada et al. 2002), $p_{\rm eff} \sim \rho G M_g/L \propto \rho^{4/3}$, provided that the mass in the volume M_g

is conserved (i.e., $\rho \propto L^{-3}$).[5] In fact, Figure 10 shows that a majority of the gas in the dense part ($\rho \gtrsim 10^{-1}\ M_\odot\ \mathrm{pc}^{-3}$) follows $p_{\mathrm{eff}} \propto \rho^{4/3}$. On the other hand, for the low-density regime, $p_{\mathrm{eff}} \propto \rho^{2/3}$. In the present model, the dominant heating source in low-density gases is shock heating. Shocks are ubiquitously generated by turbulent motion, whose velocity is ~several times 10 km s^{-1}. The kinetic energy is thermalized at shocks; then the temperature of low-density gas goes to $T_g \sim 10^4$–10^5 K. In supersonic, compressible turbulence, its energy spectrum is expected to be $E(k) \propto k^{-2}$, where the total kinetic energy $E_t = \int E(k)\, dk$. Therefore, $p_{\mathrm{eff}} \propto \rho v^2 \propto \rho^{2/3}$, because $v^2 \propto k^{-1} \propto \rho^{-1/3}$. Then the "effective" sound velocity $c_{\mathrm{eff}}^2 \equiv dp_{\mathrm{eff}}/d\rho \propto \rho^{-1/3}$ and $c_{\mathrm{eff}}^2 \propto \rho^{1/3}$ for the low- and high-density regions, respectively. This means that the effective sound velocity c_{eff} has a minimum at the transition density (ρ_t) between the two regimes. In other words, since $c_{\mathrm{eff}}^2 = c_s^2 + v_t^2$, there is a characteristic density below/above which thermal/turbulent pressure dominates the total pressure, i.e., $c_s^2 \sim v_t^2$. Thus,

$$\frac{kT_g}{\mu} \sim \frac{GM_g}{L} \sim G\rho_t L^2, \tag{15}$$

where μ is the average mass per particle and L is the size of the largest eddy of gravity-driven turbulence, which is roughly the scale height of the disk. As seen in Figure 8, the gas temperature around $\rho_0 = 10^{-1.5}\ M_\odot\ \mathrm{pc}^{-3}$ is $T_g \sim 80$ K. The scale height of the dense disk is about 10 pc (Fig. 2) in the present model; therefore,

$$\rho_t \simeq 1\ \mathrm{cm}^{-3}\left(\frac{T_g}{80\ \mathrm{K}}\right)\left(\frac{L}{10\ \mathrm{pc}}\right)^{-2}. \tag{16}$$

This transition density is close to the characteristic density in the numerical results, i.e., $\rho_0 = 10^{-1.4}$ to $10^{-1.6}\ M_\odot\ \mathrm{pc}^{-3}$ (≈2.7–1.7 cm^{-3}). In a high-density region ($\rho > \rho_t \approx \rho_0$), the stochastic nature of the system, which is the origin of the lognormality, is caused in the gravity-driven turbulence, and for low-density regions its density field is randomized by thermal motion in hot gases. For the gases around ρ_0, the random motion is relatively static; therefore, the probability of the density change is small. As a result, the density PDF takes its maximum around ρ_0. An analog of this phenomenon is a snow or sand drift in turbulent air. The material in a turbulent flow stagnates in a relatively "static" region.

As seen in Figure 2, the present gas disk has a much smaller scale height than the ISM in real galaxies, which is about 100 pc. If turbulent motion in galactic disks is mainly caused by gravitational and thermal instabilities in a rotating disk (Wada et al. 2002), we can estimate ρ_t by equation (16) in galactic disks, but the gas temperature of the dominant phase in volume is $T_g \sim 10^4$ K, as suggested by 2D models (WN01). Therefore, we expect that $\rho_t \sim 1\ \mathrm{cm}^{-3}$ is also the case in real galaxies. However, if the turbulent motion in the ISM is caused by different mechanisms, such as supernova explosions, magnetorotational instabilities, etc., the dependence of p_{eff} on density could be different from $p_{\mathrm{eff}} \propto \rho^{4/3}$, and as a result $\rho_t \sim \mathrm{const.} \sim O(1)\ \mathrm{cm}^{-3}$ could not be always true. Determining ρ_0 in a much larger disk than the present model by taking into account various physics will be an important problem for 3D simulations with a large dynamic range in the near future. In § 3.3, we compare our results with the SFR in spiral and starburst galaxies, in which ρ_0 is treated as one of the free parameters (see Fig. 12 and related discussion).

Suppose the volume-averaged density is $\langle\rho\rangle_V = 3\ M_\odot\ \mathrm{pc}^{-3}$, we can estimate the dispersion σ is $\sigma \simeq 3$ for $\rho_0 = 1\ \mathrm{cm}^{-3}$ from equation (12). For a less massive system, e.g., $\langle\rho\rangle_V = 0.3\ M_\odot\ \mathrm{pc}^{-3}$, $\sigma \simeq 2.1$. Therefore, we can expect a larger SFR for more massive systems, since the fraction of high-density gas is larger. Using this dependence of σ on the average gas density, we evaluate the global SFR in § 3.2.

3.2. *Global SFR*

Based on the numerical results in § 2 and the properties of the LN-PDF described in § 3.1, we here propose a simple theoretical model of the star formation on a global scale. We assume that the multiphase, inhomogeneous ISM in a galactic disk can be represented by a LN-PDF. Elmegreen (2002) discussed the fraction of high-density gas and the global SFR, assuming a LN-PDF. Here we follow his argument more closely.

If star formation is led by gravitational collapse of high-density clumps with density ρ_c, the SFR per unit volume, $\dot{\rho}_\star$, can be written as

$$\dot{\rho}_\star = \epsilon_c (G\rho_c)^{1/2} f_c \langle\rho\rangle_V, \tag{17}$$

where $f_c(\rho_c, \sigma)$ is the mass fraction of the gas whose density is higher than a critical density for star formation ($\rho > \rho_c$) and ϵ_c is the efficiency of star formation.

Suppose the ISM model found in § 2, whose density field is characterized by a LN-PDF, is applicable to the ISM in a galactic disk, f_c is

$$f_c(\delta_c, \sigma) = \frac{\int_{\ln \delta_c}^{\infty} \delta \exp\left[-(\ln \delta)^2/2\sigma^2\right] d(\ln \delta)}{\int_{-\infty}^{\infty} \delta \exp\left[-(\ln \delta)^2/2\sigma^2\right] d(\ln \delta)}, \tag{18}$$

$$= \frac{1}{2}\{1 - \mathrm{Erf}[z(\delta_c, \sigma)]\}, \tag{19}$$

where $\delta \equiv \rho/\rho_0$, $\delta_c \equiv \rho_c/\rho_0$, and

$$z(\delta_c, \sigma) \equiv \frac{\ln \delta_c - \sigma^2}{\sqrt{2}\sigma}. \tag{20}$$

The fraction of dense gas, f_c, is a monotonic function of δ_c and σ, and it decreases rapidly for decreasing σ. Suppose $\delta_c = 10^5$, then $f_c \sim 10^{-2}$ for $\sigma = 3.0$, and $f_c \sim 10^{-6}$ for $\sigma = 2.0$.[6] The SFR (eq. [17]) per unit volume then can be rewritten as a function of ϵ_c, δ_c, and σ:

$$\dot{\rho}_\star(\epsilon_c, \delta_c, \sigma) = \epsilon_c (G\delta_c)^{1/2} f_c \rho_0^{3/2} e^{\sigma/2}. \tag{21}$$

Using equations (12), (19), and (20), we can write the SFR as a function of the volume-averaged density $\langle\rho\rangle_V$,

$$\begin{aligned}&\dot{\rho}_\star\left[\epsilon_c, \left(\frac{\langle\rho\rangle_V}{1\ M_\odot\ \mathrm{pc}^{-3}}\right), \left(\frac{\rho_0}{1\ \mathrm{cm}^{-3}}\right), \left(\frac{\rho_c}{10^5\ \mathrm{cm}^{-3}}\right)\right]\\ &= 3.6 \times 10^{-7} \epsilon_c\ M_\odot\ \mathrm{yr}^{-1}\ \mathrm{pc}^{-3}\\ &\times \left[1 - \mathrm{Erf}\left(\frac{\ln\left(\rho_c \rho_0/\langle\rho\rangle_V^2\right)}{2\left[\ln\left(\langle\rho\rangle_V/\rho_0\right)\right]^{1/2}}\right)\right] \rho_c^{1/2} \langle\rho\rangle_V.\end{aligned} \tag{22}$$

[5] The length L is not a size of molecular clouds, but the size of the "eddies" turbulent motion in the inhomogeneous ISM. (See Fig. 2 in Wada et al. [2002] for example.) Therefore, Larson's law, i.e., $\rho \propto$ (size of molecular clouds)$^{-1}$, is not a relevant scaling relation here.

[6] In Elmegreen (2002) the dispersion of the LN-PDF, $\sigma = 2.4$, is assumed, which is taken from 2D hydrodynamic simulations of the multiphase ISM in WN01.

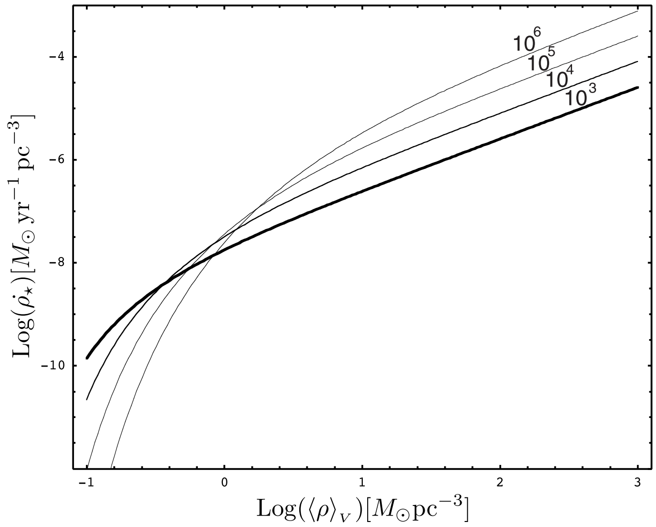

FIG. 11.—SFR ($\dot{\rho}_\star$) as a function of volume-averaged density ($\bar{\rho}$) for 0.01. We assume $\rho_0 = 1\ \mathrm{cm}^{-3}$. Four curves are plotted for $\delta_c = 10^3$ (*thick solid line*), 10^4, 10^5, and 10^6 (*from thick to thin lines*).

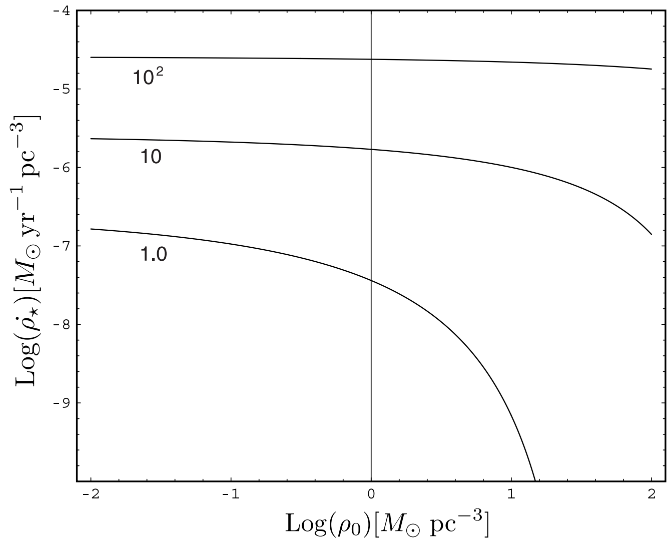

FIG. 12.—SFR ($\dot{\rho}_\star$) as a function of the characteristic density of the LN-PDF (ρ_0) for different average densities $\langle\rho\rangle_V = 10^2$, 10, and 1 $M_\odot$ pc^{-3}. We assume $\delta_c = 10^4$.

We plot equation (22) as a function of the volume-averaged density in Figure 11. Four curves are plotted for $\rho_c = 10^3$, 10^4, 10^5, and 10^6 cm^{-3}. We can learn several features from this plot. The SFR increases rapidly with increasing average density, especially for lower average density ($<1\ M_\odot$ pc^{-3}) and higher critical density. This behavior is naturally expected for star formation in the ISM described by an LN-PDF, because the dispersion σ changes logarithmically for the average gas density (eq. [12]). For large density, it approaches an SFR $\propto \langle\rho\rangle_V$. The SFR does not strongly depend on ρ_c around $\langle\rho\rangle_V \sim 1\ M_\odot$ pc^{-3}, and the SFR is larger for larger ρ_c if $\langle\rho\rangle_V > 1\ M_\odot$ pc^{-3}. This is because the free-fall time is proportional to $\rho_c^{-1/2}$, and this compensates for the decreasing fraction of high-density gas, f_c.

Figure 12 shows how SFR changes as a function of ρ_0. The SFR does not strongly depend on ρ_0 around $\rho_0 \lesssim 0.1\ M_\odot$ pc^{-3} ($\simeq 7$ cm^{-3}). See also Figure 14 in terms of comparison with the observed SFR.

3.3. *Comparison with Observations*

The theoretical SFR based on the LN-PDF in § 3.2 has a couple of free parameters. Comparison between the model and observations is useful to narrow down the parameter ranges.

We should note, however, that the gas disk presented in § 2 is geometrically thinner ($\simeq$10 pc) than real galactic disks ($\simeq$100 pc). In this sense, although the present models are based on full 3D simulations, they are not necessarily adequate for modeling typical spiral galaxies.[7] There are a couple of reasons why the present model has a small scale height. Since the disks here are relatively small ($r \simeq 1$ kpc), the disks tend to be thin due to the deep gravitational potential. Self-gravity of the gas also contributes to make the disks thin. Radiative energy loss in the high-density gas in the central region cancels the energy feedback from the supernovae (see § 4.5). Therefore, a simple way to make the model gas disks thicker to fit real galactic disks is simulating a larger disk (e.g., $r \sim 10$ kpc) with an appropriate galactic potential and supernova feedback, and solving the same basic equations.[8] Besides supernova explosions, there are other possible physical processes that could puff up the disks, such as nonlinear development of magnetorotational instability, heating due to stellar wind, and a strong radiation field from star-forming regions. These effects should be taken into account in 3D simulations with high resolutions and large dynamic ranges in the near future, and it is an important subject whether the LN-PDF is reproduced in such more realistic situations. Another interesting issue in terms of the PDF is the effect of a galactic spiral potential. However, here we try to make a comparison with observations, assuming that the LN nature in the density field found in our simulations is also the case in real galactic disks. This would not be unreasonable, because lognormality is independent of the geometry of the system. In fact a LN-PDF is also found in a 3D torus model for active galactic nuclei (AGNs) (Wada & Tomisaka 2005). A LN-PDF is naturally expected, if the additional physical processes causes nonlinear, random, and independent events that change the density field.

Figure 13 shows the surface SFR $\dot{\Sigma}_\star$ ($M_\odot$ yr^{-1} pc^{-2}) in normal and starburst galaxies (Komugi et al. 2005; Kennicutt 1998). The scale height of the ISM is assumed to be 100 pc. Four curves represent model SFRs with different critical densities. It is clear that a smaller δ_c is preferable for explaining the observations, especially for low average density. For example, an SFR with $\delta_c = 10^5$ is too steep. Similarly, Figure 14 shows the dependence of the SFR on the characteristic density ρ_0. As mentioned above, the SFR is not very sensitive to changing ρ_0, but $\rho_0 \lesssim 7.0$ cm^{-3} is better for explaining the observations. From Figure 15, the SFR is sensitive to the fraction of the LN part in volume, α, especially for low-density media. The plot implies that $\alpha = 0.01$ is too steep to fit the observations, especially for normal galaxies.

[7] One can refer to a critical study for modeling the galactic ISM using a 2D approximation (Sánchez-Salcedo 2001).

[8] This is practically difficult, if a parsec-scale spatial resolution is required. A recent study by Tasker & Bryan (2006) is almost the only work that can be directly compared with real galactic disks. Unfortunately, Tasker & Bryan (2006) do not discuss the density PDF, but they take a different approach to studying the SFR by generating "star" particles (see § 1). They claimed that a Schmidt-law–type SFR is reproduced in their simulations. This is consistent with our analysis, provided that the density PDF is LN-like and that local star formation takes place above a critical density.

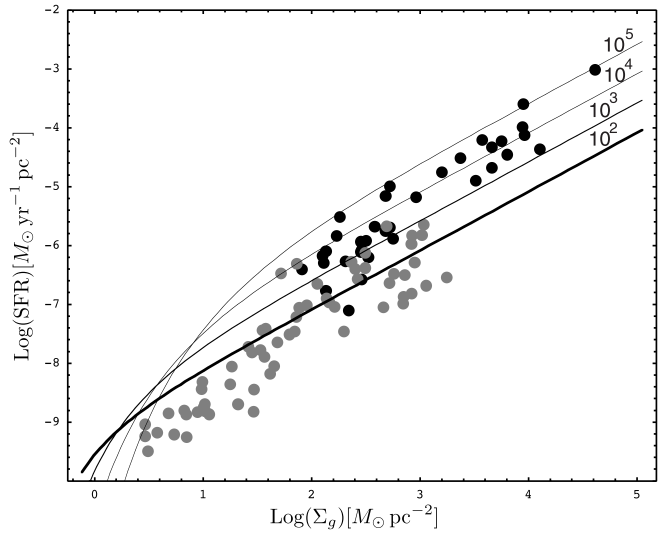

FIG. 13.—Comparison between our models and observed surface SFR in terms of surface gas density. Black dots are starburst galaxies in Kennicutt (1998), and gray dots are normal galaxies in Komugi et al. (2005). The four curves are SFRs for $\delta_c = 10^2$ (*thick solid line*), 10^3, 10^4, and 10^5. We assume $\alpha = 0.1$, $\rho_0 = 1.0$, and $\epsilon_c = 0.01$.

After exploring these parameters, we find that Figure 16 is the best-fit model with $\rho_0 = 1\ \mathrm{cm}^{-3}$, $\alpha = 0.1$ (eq. [14]), and $\delta_c = 10^3$. Three curves corresponds to SFRs with efficiency $\epsilon_c = 0.1$, 0.01, and 0.001. The model slope approaches an SFR $\propto \Sigma_g$ for large density, which is shallower than the Kennicutt law (i.e., SFR $\propto \Sigma_g^{1.41}$).

Observed SFRs in most galaxies are distributed between the model curves with $\epsilon_c \simeq 0.1$ and 0.001. The starburst galaxies are distributed in $\epsilon_c = 0.1$–0.01; on the other hand, the normal galaxies (Komugi et al. 2005) show systematically smaller SFRs, which is consistent with a smaller efficiency (i.e., $\epsilon_c = 0.01$–0.001) than those in starburst galaxies. This suggests that the large SFR in starburst galaxies is achieved by both high average gas density and large (several percent) SFE in dense clouds.[9]

[9] An alternative explanation is possible: the typical scale height of the star-forming regions is different by a factor of 10–100 in normal and starburst galaxies for the same efficiency.

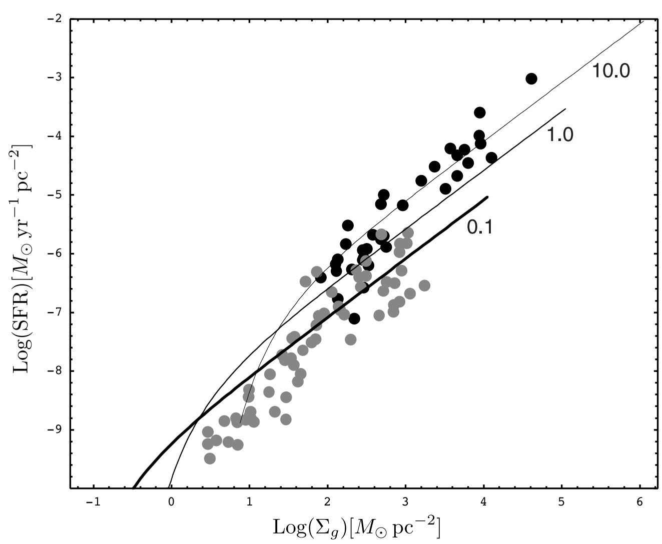

FIG. 14.—Same as Fig. 13, but for dependence of characteristic density of LN-PDF, $\rho_0 = 0.1$ (*thick solid line*), 1, and 10 $M_\odot$ pc^{-3}. We assume $\alpha = 0.1$, $\delta_c = 10^3$, and $\epsilon_c = 0.01$.

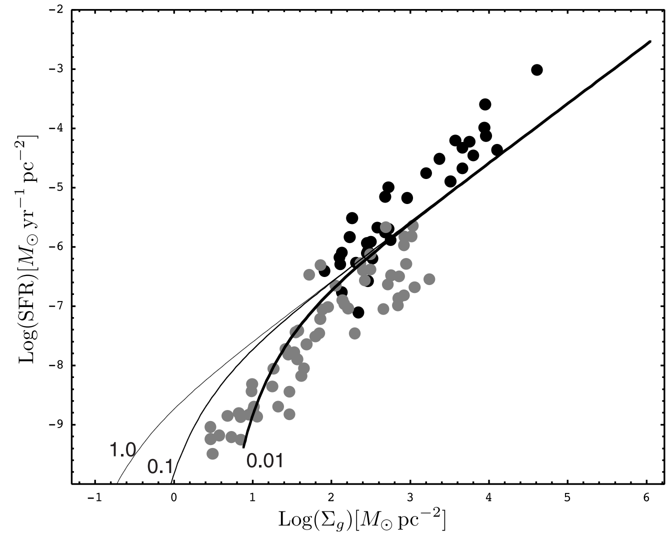

FIG. 15.—Same as Fig. 13, but for dependence of fraction of LN part, $\alpha = 0.01$ (*thick solid line*), 0.1, and 1.0. We assume $\rho_0 = 1.0$, $\delta_c = 10^3$, and $\epsilon_c = 0.01$.

Gao & Solomon (2004) found that there is a clear positive correlation between HCN and CO luminosity in 65 infrared luminous galaxies and normal spiral galaxies. They also showed that luminous and ultraluminous infrared galaxies tend to show more HCN luminosity, suggesting a larger fraction of dense molecular gas in active star-forming galaxies. Figure 17 is the SFR as a function of f_c using the model in § 3.2. Interestingly, the qualitative trend of this plot is quite similar to that of Figure 4 in Gao & Solomon (2004), which is the SFR as a function of $L_{\mathrm{HCN}}/L_{\mathrm{CO}}$ ($\propto$dense gas fraction). Both observations and our model show that the SFR increases very rapidly for increasing f_c, especially when f_c or $L_{\mathrm{HCN}}/L_{\mathrm{CO}}$ is small (<0.1), and then it increases with a power law.

4. DISCUSSION

4.1. *What Determines the Dispersion of LN-PDF?*

Elmegreen (2002) first pointed out that if the density PDF in the ISM is described by an LN function, the SFR should be a function of the critical density for local star formation and the

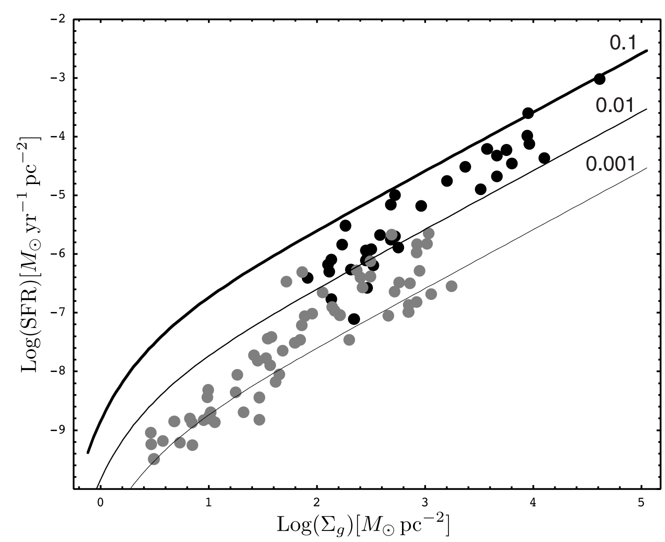

FIG. 16.—Same as Fig. 13, but for the best-fit model ($\rho_0 = 1.0$, $\alpha = 0.1$, and $\delta_c = 10^3$). The three curves are for $\epsilon_c = 0.1$ (*thick solid line*), 0.01, and 0.001.

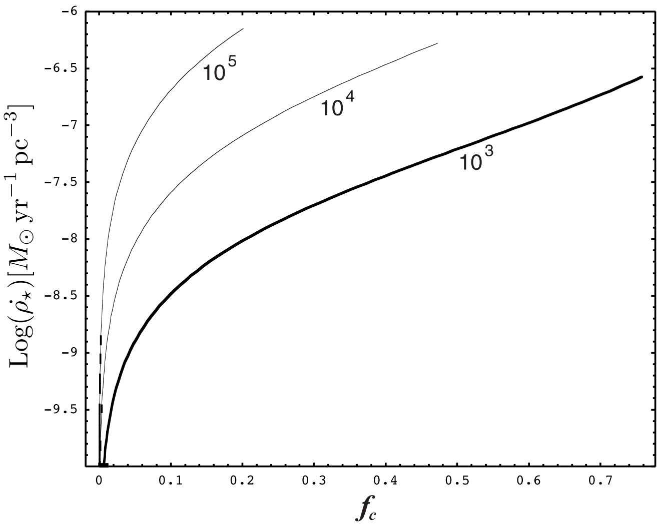

FIG. 17.—SFR as a function of fraction of high-density gas f_c. Three curves are plotted for $\delta_c = 10^3$ (*thick line*), 10^4, and 10^5. We assume $\epsilon_c = 0.1$ and $\alpha = 0.1$.

dispersion of the LN-PDF. The critical density for local star formation should be determined not only by gravitational and thermal instabilities of the ISM, but also by magnetohydrodynamic, chemical, and radiative processes on a parsec/subparsec scale. It is beyond the scope of the present paper to show how the critical density is determined. The other important parameter, σ in LN-PDF, should be related to the physics on a global scale.

Some authors claimed that the LN-PDF is a characteristic feature in an isothermal, turbulent flow, and its dispersion is determined by the rms Mach number (Vázquez-Semadeni 1994; Padoan et al. 1997; Nordlund & Padoan 1998; Scalo et al. 1998). This argument might be correct for the ISM on a local scale, for example, the internal structure of a giant molecular cloud, which is nearly isothermal and a single phase. Krumholz & McKee (2005) derived an analytic prediction for the SFR assuming that star formation occurs in virialized molecular clouds that are supersonically turbulent and that the density distribution within a cloud is LN. In this sense, their study is similar to Elmegreen (2002) and the present work. However, they assumed that the dispersion of the LN-PDF is a function of the "one-dimensional Mach number," $\mathcal{M}$, of the turbulent motion, i.e., $e^{\sigma^2} \approx 1 + 3\mathcal{M}^2/4$, which is suggested by numerical experiments of isothermal turbulence (Padoan & Nordlund 2002). A similar empirical relation between the density contrast and the magnetosonic Mach number is suggested by Ostriker et al. (2001). Yet the physical reason why the dispersion depends on the Mach number is not clear. If high-density regions are formed mainly through shock compression in a system with the rms Mach number $\mathcal{M}_{\rm rms}$, the average density contrast $\langle\delta\rho/\rho\rangle \sim \langle\rho\rangle_V/\rho_0 - 1$ could be described by $\mathcal{M}_{\rm rms}$, and it is expected that $\langle\rho\rangle_V/\rho_0 = e^{\sigma^2/2} = 1 + \mathcal{M}_{\rm rms}^2$ using equation (9). However, the ISM is not isothermal on a global scale. An inhomogeneous galactic disk is characterized by a fully developed turbulence, and its velocity dispersion is a function of scale as shown by power-law energy spectra (Wada et al. 2002). This means that the galactic disk cannot be modeled with a single "sound velocity" or velocity dispersion of the gas. Therefore, we cannot use the empirical relation of σ for galactic disks.

One should note that there is another problem with the argument based on the rms Mach number, which is in terms of the origin and mechanism of maintaining the turbulence in molecular clouds. Numerical experiments suggested that the turbulence in molecular clouds is dissipated in a sound crossing time (Mac Low 1999; Ostriker et al. 2001), and there is no confirmed prescriptions for energy sources to compensate for the dissipation. Therefore, it is more natural to assume that the velocity dispersion in a molecular cloud is not constant in a galactic rotational period, and as a result the structure of the density field is no longer static. If this is the case, taking the rms Mach number as a major parameter to describe the global SFR would not be adequate. The decaying turbulence could be supported by energy input by supernovae or outflows by protostars, but even in that case there is no clear reason to assume a uniform and time-independent Mach number.

4.2. *Observational Evidence for LN-PDF*

It is practically difficult to know the PDF of the ISM in galactic disks directly from observations. We have to map the ISM in external galaxies with fine enough spatial resolution by observational probes that cover a wide density range. The Atacama Large Millimeter/Submillimeter Array will be an ideal tool for such observations. Nevertheless, there is indirect evidence to support the LN-PDF in the Large Magellanic Cloud (LMC), which is mapped by H I with a 15 pc resolution (Kim et al. 2003) and by CO ($J = 1-0$) with 8 pc resolution (Fukui et al. 2001; Yamaguchi et al. 2001). We found that the distribution function of the H I intensity and a mass spectrum of CO clouds are consistent with a numerical model of the LMC, in which the density PDF in the simulation is nicely fitted by a single LN function (Wada et al. 2000). Although we need more information about the density field by other probes, this suggests that the entire density field of the ISM in the LMC could be modeled by a LN-PDF.

Recently, Tozzi et al. (2006) claimed that the distribution of absorption column density $N_{\rm H}$ in 82 X-ray–bright sources in the Chandra Deep Field–South is well fitted by an LN function. This suggests that the obscuring material around the AGNs is inhomogeneous, as suggested by previous numerical simulations (Wada & Norman 2002; Wada & Tomisaka 2005), and their density field is LN, if orientation of the obscuring "torus" is randomly distributed for the line of sight in the sample.

4.3. *The Q-Criterion for Star Formation*

The origin of the Schmidt-Kennicutt relation for the SFR in galaxies (Kennicutt 1998) has been often discussed in terms of gravitational instability in galactic disks. More specifically it is claimed that the threshold density for star formation can be represented by the density for which the Toomre Q parameter is unity, i.e., $Q \equiv \kappa c_s/(\pi G \Sigma_g) = 1$, where κ, c_s, and Σ_g are the epicyclic frequency, the sound velocity, and the surface density of gas, respectively (Kennicutt 1998; Martin & Kennicutt 2001). However, this is not supported by recent observations in some gas-rich spiral galaxies (Wong & Blitz 2002; Koda et al. 2005). Based on our picture described in this paper, it is not surprising that the observationally determined Q or the critical density do not correlate with the observed SFR. Stars are formed in dense molecular clouds, which are gravitationally unstable on a *local* scale (e.g., $\lesssim$1 pc), but this is basically independent of the global stability of the galactic disk. Even if a galactic gas disk is globally stable (e.g., effective $Q > 1$), cold, dense molecular clouds should exist (see also Wada & Norman 1999). Numerical results show that once the galactic disk is gravitationally and thermally unstable, inhomogeneous structures are developed, and in a nonlinear phase, it becomes "globally stable," in which the ISM is turbulent and multiphase, and its density field is characterized by an LN-PDF. In that regime, the SFR is determined by a fraction of the dense clouds and by a critical density for "local star

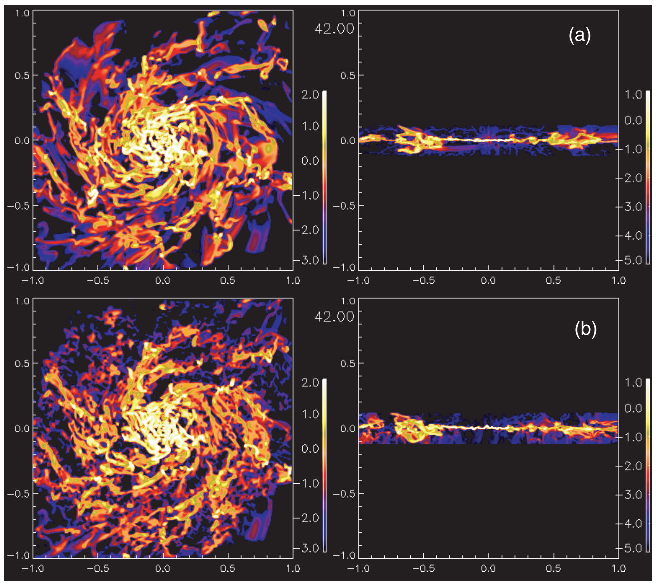

FIG. 18.—Same as Fig. 1, but for comparison between models with and without energy feedback from supernovae: (*a*) model D and (*b*) model D, but with supernova explosions at a rate of 1.5×10^{-3} yr^{-1} kpc^{-2}.

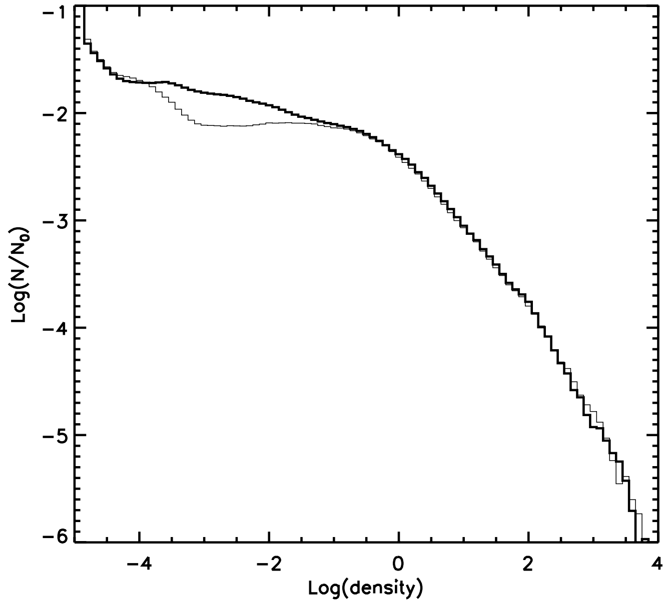

FIG. 19.—PDF in models with and without energy feedback from supernovae. The thin line is model D, and the thick line is model D, but with supernova explosions at a rate of 1.5×10^{-3} yr^{-1} kpc^{-2}.

formation,'' which should be related to physical/chemical conditions in molecular clouds, not in the galactic disk. In this picture, the SFR naturally drops for less massive systems without introducing a critical density (see Figs. 11 and 16).

Another important point, but it has been often ignored, is that the Q-criterion is derived from a dispersion relation for a *tightly wound* spiral perturbation in a thin disk with a uniform density (see, e.g., Binney & Tremaine 1987). The equation of state is simply assumed as $p \propto \Sigma^\gamma$, where Σ is the surface density and γ is a constant. The criterion for instability, i.e., $Q = 1$, means that the disk is *linearly* unstable for an *axisymmetric* perturbation. These assumptions are far from describing the star formation criterion in inhomogeneous, multiphase galactic disks. One should also note that gas disks could be unstable for nonaxisymmetric perturbations, even if $Q > 1$ (Goldreich & Lynden-Bell 1965).

Finally, we should emphasize that it is observationally difficult to determine Q precisely. All three variables in the definition of Q, i.e., surface density of the gas, epicyclic frequency, and sound velocity, are not intrinsically free from large observational errors. In particular, it is not straightforward to define the ''sound velocity,'' c_s, in the multiphase, inhomogeneous medium, and there is no reliable way to determine c_s by observations. Therefore, one should be careful of discussions based on the *absolute* value of Q in terms of a star formation criterion.

4.4. *LN-PDF and SFR in Simulations*

Kravtsov & Gnedin (2005) ran a cosmological N-body/AMR simulation to study formation of globular clusters in a Milky Way–size galaxy. They found that the density PDF in the galaxy can be fitted by an LN function and the PDF evolves with the redshift. The dispersion for the exponent of a natural log is $\sigma \simeq 1.3$, 2.0, and 2.8 at $z = 7$, 3.3, and 0, respectively. As shown in § 3.1, the dispersion of the LN-PDF is related to the average gas density in the system. Therefore, the increase of the dispersion in the galaxy formation simulation should be because of an increase of the gas density and/or a decrease of the characteristic density ρ_0. The former can be caused by accretion of the gas; in fact, Kravtsov & Gnedin (2005) show that the gas density increases until $z \simeq 5$. They also show that the characteristic density ρ_0 decreases from $z \simeq 7$ to $\simeq 3$. Based on the argument for $p_{\rm eff}$ in § 3.1, this is reasonable if (1) a clumpy, turbulent structure is developed due to gravitational instability and (2) the temperature of the lower density gas decreases due to radiative cooling with time. Qualitatively this is expected because at lower redshift, heating due to star formation and shocks caused by mergers are less effective, but radiative cooling becomes more efficient due to the increase of metallicity and gas density. Kravtsov & Gnedin (2005) mentioned that the widening LN-PDF with decreasing redshift is due to the increase of the rms Mach number of gas clouds. However, we suspect that this is not the case in formation of galactic disks (see discussion in § 4.1).

Li et al. (2006) investigated star formation in an isolated galaxy, using a 3D smoothed particle hydrodynamics (SPH) code (GADGET). They used sink particles to directly measure the mass of gravitationally collapsing gas, a part of which is considered as newly formed stars. They claimed that the Schmidt law observed in disk galaxies is quantitatively reproduced. They suggest that the nonlinear development of gravitational instability determines the local and global Schmidt laws and the SFR. Their model SFR shows a rapid decline with decreasing surface density, which is consistent with our prediction (Fig. 11).

4.5. *Effects of Energy Feedback*

In § 2, we focus on models without energy feedback from supernovae in order to know the intrinsic structure of the ISM, which is dominated by gravitational and thermal instabilities. However, one should note that the LN-PDF is robust for including energy feedback from supernovae, as suggested by previous 2D models for galactic disks and 3D models for galactic central regions (WN01 and W01). This is reasonable, because stochastic explosions in the inhomogeneous medium are a preferable situation for the LN-PDF. In order to confirm this in 3D on a galactic scale, we run a model with energy feedback from supernovae, in which a relatively large supernova rate (1.5×10^{-3} yr^{-1} kpc^{-2}) is assumed. Energy from a supernova (10^{51} ergs) is injected into one grid cell that is randomly selected in the disk. In Figures 18 and 19, we show density distributions and PDFs in models with and without energy feedback. It is clear that even for the large supernova rate the density distribution and PDF are not significantly different from the model without energy feedback, especially for the regime above the characteristic density.

4.6. *Origin of a Bias in Galaxy Formation*

It is observationally suggested that massive galaxies terminate their star formation at higher redshift than less massive galaxies, namely, "downsizing" in galaxy formation (e.g., Kauffmann et al. 2003; Kodama et al. 2004). This seems to be inconsistent with a standard hierarchical clustering scenario. It is a puzzle why the star formation timescale is shorter in more massive galaxies, in other words, why the SFR and/or the SFE are extremely biased in an environment to form massive galaxies. This might be understood by our result of the global star formation, that is, the SFR increases dramatically as a function of average gas density (Fig. 11), e.g., SFR $\propto \rho^2$ ($\rho \sim 1\ M_\odot$ pc^{-3}, for $\delta_c = 10^4$). Since the average baryon density is higher in an environment where massive galaxies could be formed, the SFR could be 100 times larger if the average gas density is 10 times higher. It would be interesting to note that this tendency is more extreme for higher critical densities (ρ_c). The critical density for star formation can be affected by UV radiation through photoevaporation of dense clouds in protogalactic halos (e.g., Susa & Umemura 2004). Qualitatively this means that for a stronger UV field, the critical density is larger; therefore, the SFR can depend strongly on the average gas density.

5. CONCLUSION

Three-dimensional, high-resolution hydrodynamic simulations of a galactic disk show that the density probability distribution function (PDF) is well fitted by a single lognormal function over six decades. The dispersion of the lognormal PDF (LN-PDF), σ, can be described by $\sigma = 1/2\ \ln(\langle\rho\rangle_M/\rho_0)$, where ρ_0 is a characteristic density and $\langle\rho\rangle_M$ is the mass-weighted average density of the ISM (eq. [13]). If all the ISM is in the regime of the LN-PDF, the star formation rate (SFR) can be represented by equation (22).

We find that the SFR is sensitive to increasing average gas density, especially for smaller $\langle\rho\rangle_V$ and larger ρ_c. However, the SFR does not significantly depend on the characteristic density ρ_0. We compare the observed SFR in normal and spiral galaxies and find that a model with $\rho_c \simeq 10^3$ cm^{-3}, a volume fraction of the LN part $\simeq 0.1$, and $\rho_0 \simeq 1$ cm^{-3} explains well the observed trend of the SFR as a function of average surface density. If the scale height of the ISM in star-forming regions is $\simeq$100 pc, the SFE in starburst galaxies is 0.1–0.01 and is 1 order of magnitude smaller in normal galaxies.

The LN nature of the density field should be intrinsic in an inhomogeneous, multiphase ISM if (1) the whole system is globally quasi-stable for a long enough period (for a galactic disk, at least a few rotational periods); (2) the system consists of many hierarchical substructures; and (3) density in such substructures is determined by random, nonlinear, and independent processes. If these conditions are satisfied, any random and nonlinear processes that affect a density field should cause an LN-PDF. In this sense, most physical processes expected in real galactic disks, such as nonlinear development of the magnetorotational instability, interactions between the ISM and stellar winds, and heating due to nonuniform radiation fields originating in OB associations, should also generate the LN-PDF. These effects on the PDF could be verified in more realistic numerical simulations with a wide dynamic range in the near future. Observational verification of the density PDF of the ISM in various phases is also desirable.

The authors are grateful to the anonymous referee for his/her careful reviewing and constructive comments. Numerical computations were carried out on a Fujitsu VPP5000 at NAOJ. K. W. is supported by Grant-in-Aids for Scientific Research (15684003 and 16204012 [K. W.]) of JSPS.

REFERENCES

Bania, T. M., & Lyon, J. G. 1980, ApJ, 239, 173
Binney, J., & Tremaine, S. 1997, Galactic Dynamics (Princeton: Princeton Univ. Press)
de Avillez, M. A. 2000, MNRAS, 315, 479
Elmegreen, B. G. 2002, ApJ, 577, 206
Fukui, Y., Mizuno, N., Yamaguchi, R., Mizuno, A., & Onishi, T. 2001, PASJ, 53, L41
Gao, Y., & Solomon, P. M. 2004, ApJS, 152, 63
Gerritsen, J. P. E., & Icke, V. 1997, A&A, 325, 972
Goldreich, P., & Lynden-Bell, D. 1965, MNRAS, 130, 125
Hockney, R. W., & Eastwood, J. W. 1981, Computer Simulation Using Particles (New York: McGraw-Hill)
Kauffmann, G., et al. 2003, MNRAS, 341, 54
Kennicutt, R. 1998, ApJ, 498, 541
Kim, S., Staveley-Smith, L., Dopita, M. A., Sault, R. J., Freeman, K. C., Lee, Y., & Chu, Y.-H. 2003, ApJS, 148, 473
Koda, J., Okuda, T., Nakanishi, K., Kohno, K., Ishizuki, S., Kuno, N., & Okumura, S. K. 2005, A&A, 431, 887
Kodama, T., et al. 2004, MNRAS, 350, 1005
Komugi, S., Sofue, Y., Nakanishi, H., Onodera, S., & Egusa, F. 2005, PASJ, 57, 733
Kravtsov, A. V. 2003, ApJ, 590, L1
Kravtsov, A. V., & Gnedin, O. Y. 2005, ApJ, 623, 650
Krumholz, M. R., & McKee, C. F. 2005, ApJ, 630, 250
Li, Y., Mac Low, M.-M., & Klessen, R. S. 2006, ApJ, 639, 879
Liou, M., & Steffen, C. 1993, J. Comp. Phys., 107, 23
Mac Low, M.-M. 1999, ApJ, 524, 169
Martin, C. L., & Kennicutt, R. C. 2001, ApJ, 555, 301
Myers, P. C. 1978, ApJ, 225, 380
Nordlund, Å., & Padoan, P. 1998, in Interstellar Turbulence, ed. J. Franco & A. Carraminana (Cambridge: Cambridge Univ. Press), 218
Ostriker, E. C., Stone, J. M., & Gammie, C. F. 2001, ApJ, 546, 980
Padoan, P., & Nordlund, Å. 2002, ApJ, 576, 870
Padoan, P., Nordlund, Å., & Johns, B. J. T. 1997, MNRAS, 288, 145
Rosen, A., & Bregman, J. N. 1995, ApJ, 440, 634
Sánchez-Salcedo, F. J. 2001, ApJ, 563, 867
Scalo, J., Vázquez-Semadeni, E., Chappell, D., & Passot, T. 1998, ApJ, 504, 835
Schmidt, M. 1959, ApJ, 129, 243
Slyz, A. D., Devriendt, J. E. G., Bryan, G., & Silk, J. 2005, MNRAS, 356, 737
Spaans, M., & Norman, C. 1997, ApJ, 483, 87
Susa, H., & Umemura, M. 2004, ApJ, 610, L5
Tasker, E. J., & Bryan, G. L. 2006, ApJ, 641, 878
Tozzi, P., et al. 2006, A&A, 451, 457
van Leer, B. 1979, J. Comp. Phys., 32, 101
Vázquez-Semadeni, E. 1994, ApJ, 423, 681
Vázquez-Semadeni, E., Gazol, A., & Scalo, J. 2000, ApJ, 540, 271
Wada, K. 2001, ApJ, 559, L41 (W01)
Wada, K., Meurer, G., & Norman, C. A. 2002, ApJ, 577, 197
Wada, K., & Norman, C. A. 1999, ApJ, 516, L13
———. 2001, ApJ, 547, 172 (WN01)
———. 2002, ApJ, 566, L21
Wada, K., Spaans, M., & Kim, S. 2000, ApJ, 540, 797
Wada, K., & Tomisaka, K. 2005, ApJ, 619, 93
Wong, T., & Blitz, L. 2002, ApJ, 569, 157
Yamaguchi, R., et al. 2001, PASJ, 53, 985